IEEE Photonics Journal
An IEEE Photonics Society Publication

Open Access

On the *m*-CAP Performance with Different Pulse Shaping Filters Parameters for Visible Light Communications

Volume 9, Number 5, October 2017

Petr Chvojka
Khald Werfli
Stanislav Zvanovec
Paul Anthony Haigh
Vaclav Hubata Vacek
Petr Dvorak
Petr Pesek
Zabih Ghassemlooy

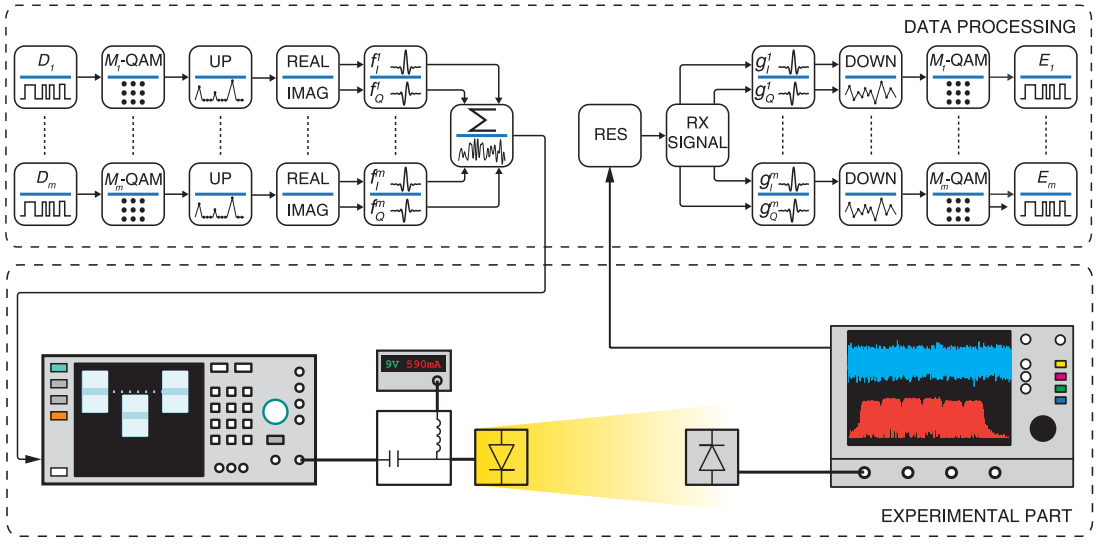

DOI: 10.1109/JPHOT.2017.2749203
1943-0655

On the *m*-CAP Performance with Different Pulse Shaping Filters Parameters for Visible Light Communications

Petr Chvojka,[1] Khald Werfli,[2] Stanislav Zvanovec,[1] Paul Anthony Haigh,[3] Vaclav Hubata Vacek,[1] Petr Dvorak,[1] Petr Pesek,[1] and Zabih Ghassemlooy[2,4]

[1]Department of Electromagnetic Field, Faculty of Electrical Engineering, Czech Technical University in Prague, Prague 16627, Czech Republic
[2]Optical Communications Research Group, Northumbria University, Newcastle upon Tyne NE1 8ST, U.K.
[3]Department of Electronic and Electrical Engineering, University College London, London WC1E 6BT, U.K.
[4]QIEM, Chinese Academy of Sciences, Fujian 350002, China

DOI:10.1109/JPHOT.2017.2749203

Manuscript received August 11, 2017; revised August 31, 2017; accepted August 31, 2017. Date of publication September 4, 2017; date of current version September 27, 2017. This work was supported in part by GACR 17-17538S, in part by CTU Grant SGS17/182/OHK3/3T/13, and in part by the U.K. ESPRC Grant EP/P006280/1: Multifunctional Polymer Light-Emitting Diodes with Visible Light Communications (MARVEL). Corresponding author: Petr Chvojka (e-mail: chvojpe8@fel.cvut.cz).

Abstract: In pulse shaping filters, parameters such as the roll-off factor and the symbol span, which determine the overall performance, are of great importance when implementing a real-time system due to limited hardware resources. In this paper, we experimentally investigate a multiband carrier-less amplitude and phase (*m*-CAP) visible light communications (VLC) system employing such filters and assess the link performance for a range of filter lengths and show the relationship between the system data rate (or spectral efficiency) and computational complexity. We show that lower order *m*-CAP can offer the same system performance as higher order systems while offering much lower computational complexity. By optimizing the filter parameters and the order m of an *m*-CAP VLC link, we achieve the largest improvement in the data rate and bandwidth efficiency of 9.69% and 40.43%, respectively, when compared with 2- and 8-CAP. We also show that the *m*-CAP VLC link with $m \geq 6$ can be designed with the same filter parameters to demonstrate a link with both the highest data rate and spectral efficiency simultaneously in contrast to lower order systems.

Index Terms: Multiband carrier-less amplitude and phase modulation, pulse shaping filters, visible light communications.

1. Introduction

Recently, radio frequency (RF) based wireless spectrum has become a valuable commodity due to the exponentially increasing demand for very high-speed internet access [1]. As a result, spectrum congestion, which affects the availability of high-speed internet services, has become an issue that needs to be addressed [2]. Optical wireless communications (OWC), which is most suitable for indoor environments, is an alternative and complementary technology to RF, appropriate to overcome spectral challenges offering unregulated and high bandwidth (in the orders of THz). Over the last decade, visible light communications (VLC), as a part of OWC, has undergone rapid

development, exploiting advantages from solid-state lighting (SSL) technologies with high-speed switching capabilities [2]. VLC utilizes white light-emitting diodes (LEDs) to provide illumination and high-speed data transmission simultaneously for a range of applications including broadcasting, indoor positioning, and vehicular or underwater communications [2]. Despite the benefits of LEDs (i.e., energy efficiency and longer lifetime), they introduce a major system drawback due to the very low modulation bandwidths available, in the order of few MHz [2]. This impediment is caused by the long recombination times of cerium-doped yttrium aluminium garnet (Ce:YAG) phosphors used for colour conversion to create a white light.

The vast majority of studies have focused on implementation of advanced techniques to achieve higher data rates and spectrally efficient communication links such as: *i*) blue filtering that suppresses the slow phosphor layer; thus increasing the LED bandwidth up to 20 MHz [3], *ii*) pre- and post-equalization [4], [5]; *iii*) utilizing multiple LEDs via wavelength-division multiplexing (WDM) and spatial-multiplexing known as multiple-input multiple-output (MIMO) [6]; *iv*) advanced modulation schemes such as carrier-less amplitude and phase modulation (CAP) [7] and orthogonal frequency division multiplexing (OFDM) [8], [9].

The modulation formats outlined above provide a straightforward approach for increasing the link capacity, especially in bandlimited environments. Recently, optical OFDM VLC links with data rates $>$ 5 Gb/s based on a single blue μLED and WDM technique have been reported in [10] and [11], respectively. The key advantage of OFDM lies in the possibility to optimise the system performance based on the channel parameters by means of bit- and power-loading algorithms [12]. On the other hand, the main drawback of OFDM is the high peak-to-average power ratio (PAPR) due to the summation of a high number of subcarrier signals to high signal peaks [13], making OFDM systems sensitive to the devices with the nonlinear electro-optics characteristics such as amplifiers and LEDs. Many techniques have been proposed to reduce PAPR including employing pilot symbols (PS) [14], linearization of the LED response [15], or encoding transmit data symbols including DC biasing [16].

As an alternative solution, CAP is conceptually simpler and has lower PAPR compared with OFDM [17]. However, the CAP modulation scheme requires a flat frequency response, which is seldom available in VLC, in order to effectively implement it. To increase the link performance of systems with a non-flat frequency response, a complex equalizer is needed [18]. In [19] a solution to overcome the flat band requirement was introduced by the way of splitting the available signal bandwidth into *m* sub-bands (or subcarriers) thus resulting in multiband CAP (*m*-CAP). Such an approach enables to relax the flat-band response requirement by allocating a narrow bandwidth to individual subcarriers, thus the frequency flatness can be easily achieved. Moreover, it enables bit- and power-loading by adjusting the number of bits-per-symbol or the power level of individual subcarriers. Note that, increasing *m* leads to improvement of the transmission speed due to the lower attenuation of each subcarrier induced by an LED frequency response as was shown in [20]. In *m*-CAP schemes finite impulse response (FIR) pulse shaping filters are utilized to generate carrier frequencies introducing most of the complexity. Thus, the multiband approach can significantly increase the computational complexity of the system by requiring 2*m* FIR filters at the transmitter and additional 2*m* FIR filters at the receiver, thus resulting in 4*m* filters in total.

In our previous works, we investigated *m*-CAP VLC performance in VLC via numerical simulations [21], [22] and experimental measurements [20], [23]. Firstly, in [19] we showed an experimental VLC link over a 1 m distance with a high spectral efficiency 4.85 b/s/Hz, demonstrating promising results for the following research. In our most recent works, *m*-CAP was tested using MATLAB simulations. For instance, a new concept of *m*-CAP utilizing unequally distributed subcarriers was introduced showing both reduced computational complexity and higher achievable data rates [24], [25]. However, such a scheme has greater requirements for a flat-band response due to the high bandwidth allocated to the first subcarrier, which is set within passband region of an LED. The system performance in a highly bandlimited environment was investigated in [26], and it was shown that *m*-CAP could significantly outperform a traditional 1-CAP scheme in terms of the achievable data rate (by up to 40%). Nevertheless, none of these reports did consider the length of the pulse shaping filters. This is because filters were not a crucial in the investigation, and since they

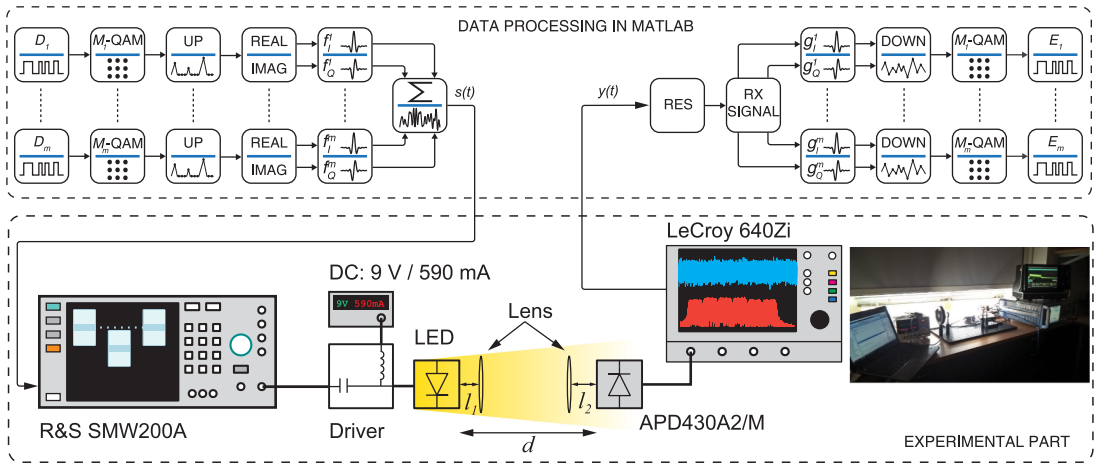

Fig. 1. The schematic block diagram of the *m*-CAP VLC system. Inset is a photo of the experimental link. Note that, 'UP', 'RES' and 'DOWN' blocks refers to up-sampling, resampling and down-sampling, respectively.

were offline systems with no practical limits on the number of filter taps that could be used, which is an issue in real time systems. However, in a real implementation, the filter parameters such as the roll-off factor and the symbol span significantly impact the system performance [27]. Increasing both parameters leads to a lower bit error rate (BER) performance at the cost of increased computational complexity, which is a major issue in the implementation of *m*-CAP on field programmable gate arrays (FPGAs) due to the limited hardware resources.

Therefore, in this paper, we build on our previous work in [27] and experimentally investigate in considerable detail, the performance of the *m*-CAP VLC system for a range of FIR filter conditions to understand the physical performance of the system. We set the filter parameters within given ranges in terms of the roll-off factor β, symbol span L_s for the set of subcarriers m, and demonstrate how these parameters influence both the measured bit rates and spectral efficiencies. We focus on the dependence of data rate and spectral efficiency on the filter parameters and system complexity, then show how these parameters trade-off enables to achieve an optimum *m*-CAP VLC hardware implementation. The paper focuses on the *m*-CAP VLC link performance with no equalisation schemes, although further performance gains could be expected with equalization.

2. System Setup

The schematic block diagram of the system under test is illustrated in Fig. 1, showing both the *m*-CAP generation in MATLAB and, the experimental set-up with a photo from the experiment inset. Firstly, a $2^{15} - 1$ pseudorandom binary sequence (PRBS) D_m is generated for each subcarrier and the bits are then mapped onto an *M*-ary quadrature amplitude modulation (*M*-QAM) constellation, where $M = 2^k$ is the order of QAM and k is the number of bits/symbol. The data is up-sampled using the normal zero-padding method with the following number of zeros-per-symbol, according to [19], [20]:

$$n_s = 2 \cdot \lceil 2m(1+\beta) \rceil \tag{1}$$

where $\lceil \cdot \rceil$ is the ceiling function. Next, the data is split into the real (in-phase *I*) and imaginary (quadrature *Q*) parts prior to being passed through the pulse shaping square-root-raised cosine (SRRC) filters. The impulse responses of the transmit filters are given as a product of the SRRC filter impulse responses and sine (*Q*) and cosine (*I*) waves forming a Hilbert pair for the *I* and *Q*

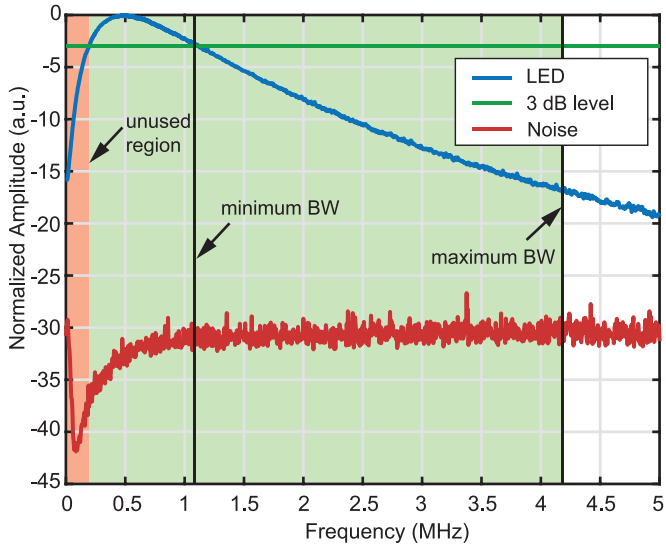

Fig. 2. The measured LED frequency response showing the unused low frequencies and minimum and maximum available signal bandwidths. Also shown the noise spectrum.

filters, respectively as given by [20], [27]:

$$f_I^m(t) = \frac{\sin(\gamma(1-\beta)) + 4\beta\frac{t}{T_s}\cos(\gamma\delta)}{\gamma[1-(4\beta\frac{t}{T_s})^2]}\cos[\gamma(2m-1)\delta] \tag{2}$$

for the *I* filter and

$$f_Q^m(t) = \frac{\sin(\gamma(1-\beta)) + 4\beta\frac{t}{T_s}\cos(\gamma\delta)}{\gamma[1-(4\beta\frac{t}{T_s})^2]}\sin[\gamma(2m-1)\delta] \tag{3}$$

for the *Q* filter, where T_s is the symbol duration, $\gamma = \pi t/T_s$ and $\delta = 1+\beta$. The output signal of the *m*-CAP transmitter is given by [20], [27]:

$$s(t) = \sqrt{2}\sum_{n=1}^{m}(s_I^n(t) \otimes f_I^n(t) - s_Q^n(t) \otimes f_Q^n(t)), \tag{4}$$

where $s_I^n(t)$ and $s_Q^n(t)$ are *I* and *Q* *M*-QAM symbols for the n^{th} subcarrier and $\otimes$ represents the time domain convolution.

The output signal $s(t)$ is loaded into a Rohde & Schwarz SMW200A vector signal generator (with the maximum sampling rate 200 MSa/s) and passed through the custom-built LED driving circuit for intensity modulation of the LED. We used the commercially available LED (OSRAM Golden Dragon) biased at $\sim$ 590 mA to ensure the operation in its most linear region. The measured LED frequency response is illustrated in Fig. 2 showing the 3 dB modulation bandwidth at 1.2 MHz (with a cut-on frequency of 0.2 MHz). For the experiment, we shifted the signal in the frequency domain by 0.2 MHz due to the significant signal distortion caused by the non-flat frequency response of the LED (denoted by the red region in Fig. 2). By varying β from 0.1 to 1, the signal bandwidth requirements are changed according to $B_{tot} = B_{sig}(1+\beta)$, where B_{sig} is the signal bandwidth set in this work to $\{1, 2\}$ MHz. Thus, the minimum and maximum total signal bandwidth B_{tot} were 1.1 MHz and 4.2 MHz, respectively, as highlighted in Fig. 2. The reason for choosing such a low B_{sig} is to ensure the optimal system performance during the measurement even for the maximum B_{tot}, which is $\sim$ 4 times higher than minimum B_{tot}.

The transmission distance *d* between the LED and the avalanche photodetector (PD) (Thorlabs APD430A2/M) based receiver was set to 1 m. Two 25.4 mm biconvex lenses were placed at distances of $l_1 = 0.25$ m and $l_2 = 0.35$ m from the LED and the PD, respectively, for beam collimation

TABLE 1
SNR Thresholds for BER Target 10^{-3}

k	**1**	**2**	**3**	**4**	**5**
SNR (dB)	6.8	9.8	14.4	16.5	20.6
k	**6**	**7**	**8**	**9**	
SNR (dB)	22.6	26.5	28.4	32.3	

and focusing, see Fig. 1. At the receiver, the regenerated electrical signal was captured using real time oscilloscope (LeCroy WaveRunner Z640i with 2 GSa/s sampling rate) for further offline data processing in MATLAB.

The received signal is given as:

$$y(t) = \Re G\, s(t) \otimes h(t) + n(t), \tag{5}$$

where $h(t)$ is the channel impulse response, $\Re$ and G are the PD's responsivity and gain, respectively and $n(t)$ is the additive white Gaussian noise (AWGN) with zero mean and variance of $N_0/2$, where N_0 is power spectral density. The received signal $y(t)$ was resampled to have the same sampling frequency as $s(t)$ and passed through time-reversed receive filters g_I (in-phase) and g_Q (quadrature) matched to the transmit filters as $g_I^m(t) = f_I^m(-t)$ and $g_Q^m(t) = f_Q^m(-t)$. Following down-sampling and demodulation, the *M*-QAM symbols are recovered and the received bits are compared with the transmitted data and the link BER is determined by aggregating BER values from every subcarrier. To maximize system performance, a bit-loading technique was applied as follows. A binary phase shift keying (BPSK) pilot signal was transmitted to measure the root-mean-square error vector magnitude (EVM_{RMS}) for individual subcarriers. Based on the signal to noise ratio (SNR), defined as $SNR = 20\log_{10}(EVM_{RMS})$, the appropriate number of bits/symbol $k = \{1, 2, 3, 4, 5, 6, 7, 8, 9\}$ was loaded into each subcarrier based on the SNR threshold levels listed in Table 1 for a target BER of 10^{-3}, which is slightly below the forward error correction (FEC) limit with an overhead of 7%, and in consistency with our previous works [20], [21], [23]. The SNR thresholds can be found in the literature [28]. The example of the measured SNR against the subcarrier index for $L_s = 10$, $\beta = 0.2$ and $m = \{2, 4, 6, 8, 10\}$ for a range of *M*-QAM is illustrated in Fig. 3. Also depicted are SNR threshold levels for *M*-QAM modulations.

3. Results and Discussion

As previously outlined, the goal of this paper is to show the relationship between the FIR filter parameters and the VLC system performance. The length (number of taps) of the filters, which introduces major system complexity, is given by three main parameters: *(i)* $L_s = \{2, 4, 6, 8, 10\}$; *(ii)* $\beta = \{0.1, 0.2, 0.3, 0.4, 0.5, 0.6, 0.7, 0.8, 0.9, 1\}$; and *(iii)* $m = \{2, 4, 6, 8, 10\}$. The reason for setting a value of L_s up to 10 is based on our previous research [27]. We showed that utilizing $L_s > 12$ is impractical due to no additional performance improvement. However, increasing L_s from 10 to 12 brings only slight enhancement in the system performance while system complexity is increased substantially. Thus, here we set $L_s = 10$ as a maximum analysed value. In the experiments described below, B_{sig} is set to 1 MHz unless otherwise stated. The achieved results are discussed in terms of the measured bit rate R_b, spectral efficiency η_{se} and filter length L_f (taps/filter) over the entire range of L_s and β. We will focus particularly on $m = \{2, 6, 8, 10\}$, detailed discussion on $m = 4$ will be limited due to their similar performances. The comparison with a 1-CAP system is not included here, since we have already shown in our previous reports that *m*-CAP significantly

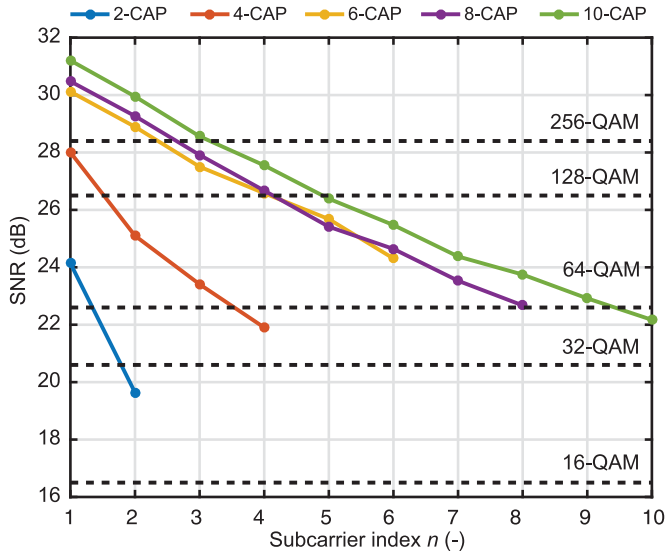

Fig. 3. The measured SNR against the subcarrier index using a BPSK pilot signal for $L_s = 10$, $\beta = 0.2$, $m = \{2, 4, 6, 8, 10\}$ and a range of *M*-QAM. Also depicted are SNR thresholds for different *M*-QAM signals (dashed line).

outperforms a 1-CAP scheme [20], [21], [26]. The achieved R_b was determined in the same manner as BER, i.e., as the sum of the transmission speeds from individual subcarriers.

3.1 2-CAP

The measured R_b, η_{se} and corresponding L_f are illustrated in Fig. 4(a), (b), and (c), respectively. Increasing both filter parameters L_s and β improves the measured R_b significantly from 1 Mb/s to 6.5 Mb/s (the highest R_b for 2-CAP in this work), thus having approximately the same impact on the measured R_b and η_{se}, see Fig. 4(a). However, the effect on η_{se} is different as can be seen from Fig. 4(b). For low values of $L_s = 4$ and $L_s = 2$, η_{se} is increased slowly or remains almost constant over the range of β, respectively. The effect of β is much more significant for $L_s > 4$ showing at first a rapid improvement in η_{se} up to 4.23 b/s/Hz in case of $\beta = 0.3$ and $L_s = 10$ (the highest η_{se} in 2-CAP) due to the higher bandwidth allocated to individual subcarriers, which are however not significantly attenuated by the LED response. Nevertheless, for $\beta > 0.3$ and > 0.5 and for $L_s = 10$ and 8, we notice degradation in the measured η_{se}. The performance degradation in η_{se} is caused by the increasing bandwidth requirement of the subcarriers, which are more prone to the frequency dependent attenuation caused by the LED frequency response. Moreover, the higher the bandwidth is the flat-band response approximation is decreased. It is clear from Fig. 4(a) and (b) that 2-CAP system can be designed either for the highest R_b or η_{se}, which introduces a substantial drawback in comparison to higher order *m*-CAP systems.

Fig. 4(c) illustrates the corresponding length of filters L_f as a function of β and for a range of L_s. Also shown are the received constellation diagrams for subcarriers n_1 and n_2 for the case of the most bandwidth efficient 2-CAP (i.e., $\beta = 0.3$, $L_s = 10$) with L_f of 120 taps/filter requirement. Note that, higher values of β and L_s will lead to increasing system complexity. As can be seen, L_f is increased more rapidly with L_s for a fixed value of β reaching up to ~ 5 times higher number of taps (for $\beta = 1$), in contrast to the case of a fixed L_s and increasing β where complexity raises up to ~ 1.6 times (for $L_s = 10$). Note, some parts of the individual curves remain constant over the range of β (e.g., from 0.3 to 0.5 for all values of L_s), which means that increasing β does not necessarily lead to longer filters. Therefore, higher computational complexity can be avoided, which is desirable in real time implementation of the link. This introduces an unexpected advantage over the higher order *m*-CAP systems. As will be seen later, the higher order *m*-CAP links (in this work

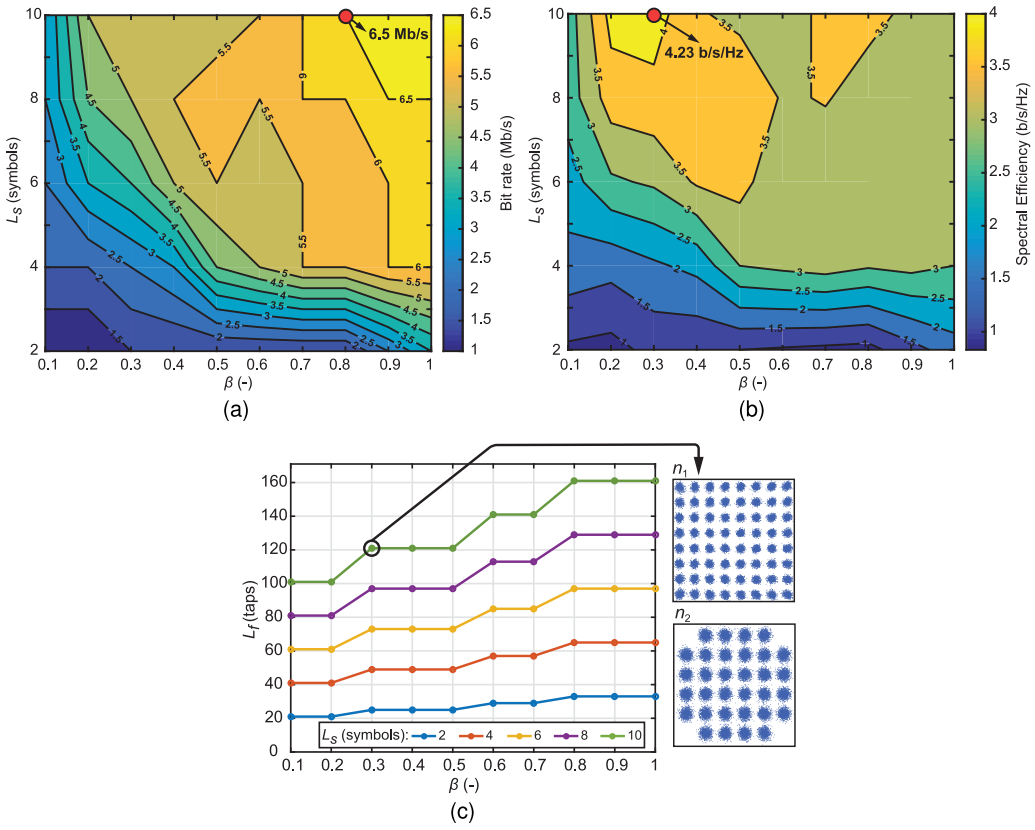

Fig. 4. Experimentally measured: (a) data rates, (b) spectral efficiencies and (c) corresponding filter lengths for 2-CAP with the received constellation diagrams for subcarriers n_1 and n_2 for $L_s = 10$ and $\beta = 0.3$. Note that a red dot in (a) and (b) denotes the highest measured data rate and spectral efficiency.

$m \geq 6$) can be optimized for both the highest bit rate and spectral efficiency using the same FIR filter parameters, i.e. the given value of L_s and β.

3.2 6-CAP

The measured R_b and η_{se} and appropriate L_f for 6-CAP against a range of β are depicted in Fig. 5(a), (b), and (c), respectively. As expected, both filter parameters have the same impact on the measured R_b as in the previous case, see Fig. 4(a). However, to achieve the optimal R_b (i.e., $>$ 6.5 Mb/s in this case) the values of $L_s \geq 4$ and $\beta \geq 0.6$ should be set, thus allowing a far greater degree of freedom in a system design compared to the 2-CAP system. For 6-CAP, the highest measured R_b is 7 Mb/s for $\beta = 0.3$ and $L_s = 10$. Note that, the impact of β is more distinctive for $L_s \geq 4$. At first, R_b is rapidly increasing to $>$ 6.5 Mb/s for $L_s = \{4, 6, 8, 10\}$ and corresponding $\beta = \{0.6, 0.4, 0.3, 0.2\}$. Further increase of β does not improve the link capacity significantly since the transmission speed is within the range of 6.5 to 7 Mb/s. However, we notice a slight decrease in R_b for $L_s = 4$ and $\beta > 0.6$.

The measured η_{se} as a function of β is illustrated in Fig. 5(b), showing similar behaviour to the 2-CAP system. Nevertheless, increasing both L_s and β have a higher impact on the system as higher improvement in η_{se} can be expected. The highest η_{se} of 5.83 b/s/Hz was measured for $\beta = 0.2$ and $L_s = 10$. For $L_s > 4$, increasing β beyond a certain value (e.g., $L_s = 6$ and $\beta > 0.5$) leads to a system performance degradation in terms of η_{se} as the individual subcarriers with higher bandwidth requirement are more prone to higher frequency attenuation. Fig. 5(c) depicts L_f as a function of β, for a range of L_s. The insets show the received constellation diagrams for the first n_1 and third n_3 subcarriers with $L_f = 300$ taps/filter for the most bandwidth efficient configuration of 6-CAP (i.e., with $\beta = 0.2$ and $L_s = 10$). Clearly, L_f increases with L_s for a given value of β. For instance, for

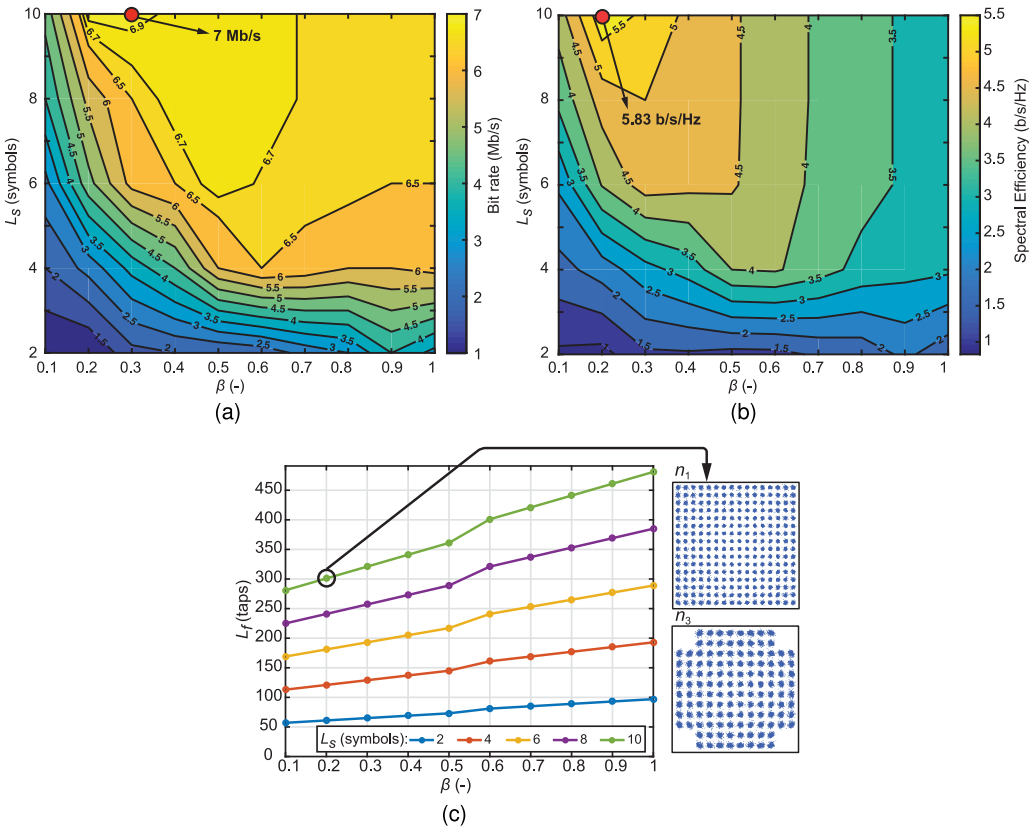

Fig. 5. Experimentally measured: (a) data rates, (b) spectral efficiencies and (c) corresponding filter lengths for 6-CAP with the received constellation diagrams for subcarriers n_1 and n_3 for $L_s = 10$ and $\beta = 0.2$. Note that a red dot in (a) and (b) denotes the highest measured data rate and spectral efficiency.

$\beta = 1$ the value of L_f is increased by over 4 times when L_s is changed from 2 to 10. In contrast to 2-CAP, where we can reach either R_b or η_{se} to be maximal, here a link with both the highest R_b and η_{se} can be can be designed for a single system setup, i.e. $\beta = 0.2$ and $L_s = 10$.

To illustrate further the performance of the system, B_{sig} was increased to 2 MHz and the measured R_b and η_{se} for 6-CAP are depicted in Fig. 6(a) and (b), respectively. As can be seen, the optimum R_b and η_{se} are observed within $0.3 < \beta < 0.6$ and $0.2 < \beta < 0.4$, respectively. Note that, the highest measured R_b and η_{se} are 11.33 Mb/s ($L_s = 10$ and $\beta = 0.4$) and 4.31 b/s/Hz ($L_s = 10$ and $\beta = 0.2$), respectively. By increasing B_{sig} we achieved $\sim$ 62% improvement in maximum measured R_b in 6-CAP system but the highest η_{se} decreased by $\sim$ 26%. This is due to the higher bandwidth of individual subcarriers, which are more prone to the attenuation outside the LED modulation bandwidth.

3.3 8-CAP

Fig. 7(a) and (b) illustrate the measured R_b and η_{se} for the 8-CAP system, respectively, showing a similar profile to the previous 6-CAP case. The optimal $R_b > 6.5$ Mb/s was measured in two separate regions. The ripple is caused by optimal subcarrier allocation within the LED frequency response. However, the significant performance degradation in η_{se} should be expected for the region where $\beta = \{0.7, 0.8, 0.9\}$, compared to lower β values, see Fig. 7(b). The highest $R_b = 7.14$ Mb/s and $\eta_{se} = 5.94$ b/s/Hz in 8-CAP (both are the highest measured values in this work for $B_{sig} = 1$ MHz) were measured for $L_s = 10$ and $\beta = 0.2$.

The corresponding filter tap requirement L_f as a function of L_s and β is illustrated in Fig. 7(c) with the received constellation diagrams for the first n_1 and fourth n_4 subcarriers inset. For the best performing filter setup, i.e. $L_s = 10$ and $\beta = 0.2$, a single filter requires $L_f = 401$ taps/filter, which

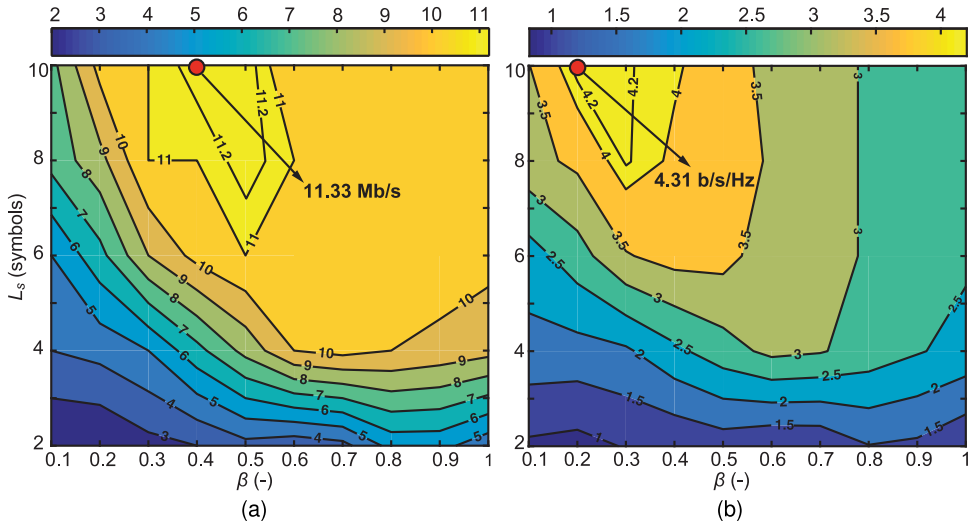

Fig. 6. The measured: (a) bit rate and (b) spectral efficiency for 6-CAP link for $B_{sig} = 2$ MHZ. Compared to $B_{sig} = 1$ MHz, higher data rate and lower bandwidth efficiency were measured. Note that a red dot in (a) and (b) denotes the highest measured data rate and spectral efficiency.

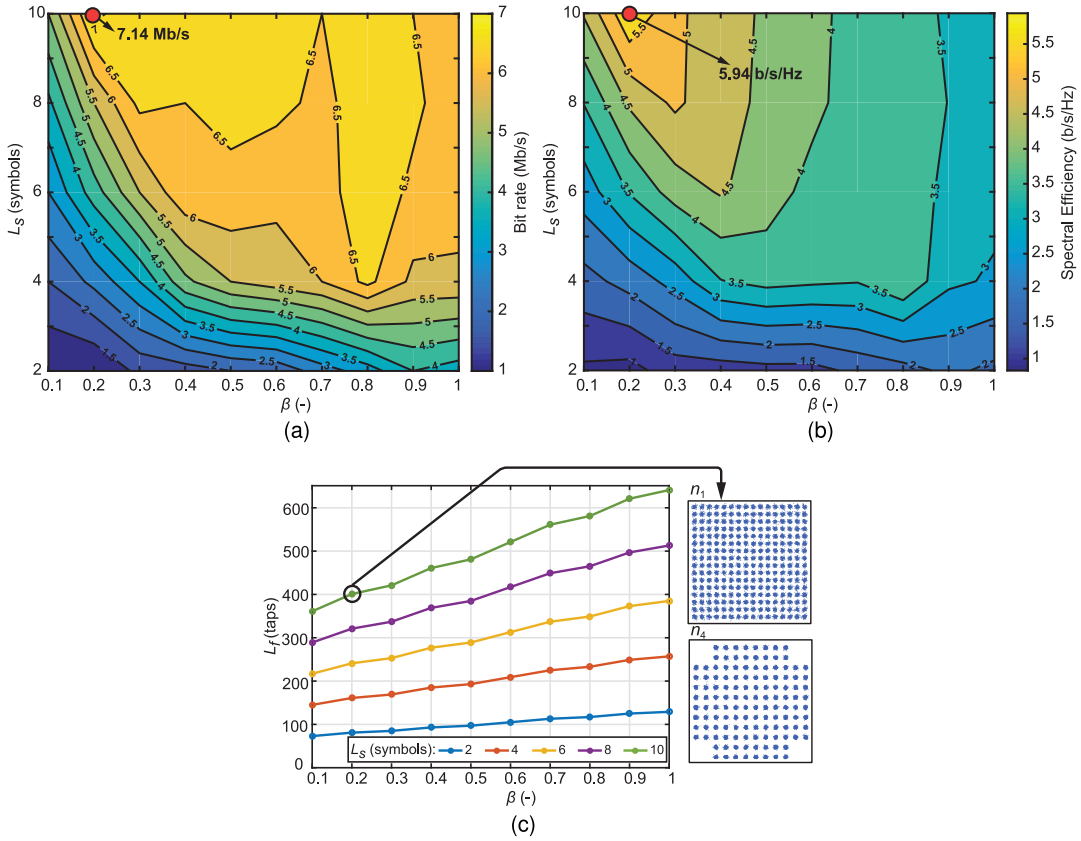

Fig. 7. Experimentally measured: (a) data rates, (b) spectral efficiencies and (c) filter lengths for 8-CAP with the received constellation diagrams for subcarriers n_1 and n_4 for $L_s = 10$ and $\beta = 0.2$. Note that a red dot in (a) and (b) denotes the highest measured data rate and spectral efficiency.

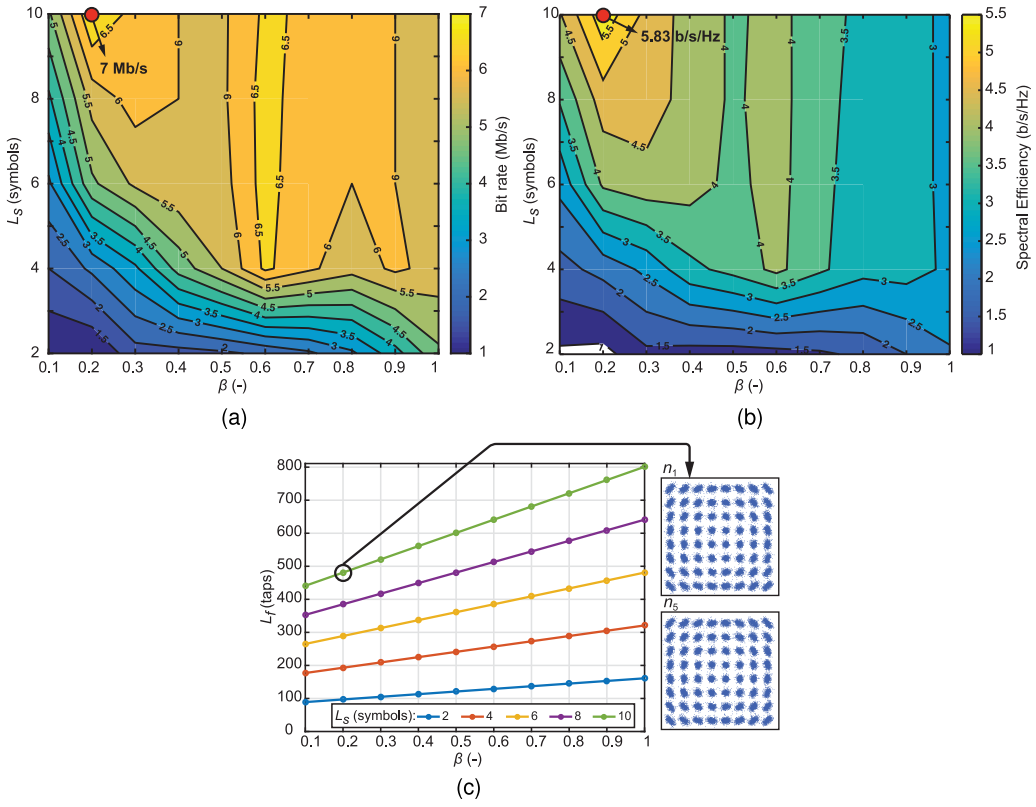

Fig. 8. Experimentally measured: (a) data rates, (b) spectral efficiencies and (c) filter lengths for 10-CAP with the received constellation diagrams for subcarriers n_1 and n_5 for $L_s = 10$ and $\beta = 0.2$. Note that a red dot in (a) and (b) denotes the highest measured data rate and spectral efficiency.

substantially increases the overall system complexity. On the other hand, to keep the optimal value of $R_b > 6.5$ Mb/s, the computational complexity can be reduced by $\sim 31\%$, i.e. from $L_f = 337$ taps/filter ($L_s = 8$ and $\beta = 0.3$) to $L_f = 233$ taps/filter ($L_s = 4$ and $\beta = 0.8$). The corresponding measured η_{se} is then reduced by 30% from 5 b/s/Hz to 3.5 b/s/Hz, see Fig. 7(a) and (b).

3.4 10-CAP

For 10-CAP the measured R_b and η_{se} are illustrated in Fig. 8(a) and (b), respectively showing similar profiles to 2- and 6-CAP systems. However, R_b is $>$ 6.5 Mb/s was measured for two separated maxima for $\beta = 0.2$ and 0.6, which is because of optimal subcarrier allocation within to the LED frequency response. Note that, the loss of η_{se} should be expected around $\beta = 0.6$ when compared to the $\beta = 0.2$ case. The maximum measured R_b and η_{se} are 7 Mb/s and 5.83 b/s/Hz for $L_s = 10$ and $\beta = 0.2$, which is the same as in 6-CAP link but higher than 2-CAP. Therefore, we observe no additional improvement in both R_b and η_{se} when a high number of subcarriers (i.e., $m \geq 6$) is used in *m*-CAP system because of low B_{sig}. The value of $L_f = 481$ taps/filter for such a 10-CAP system introduces a redundant increase of the system complexity. Fig. 8(c) illustrates the filter taps requirement for a range of β and L_s (inset are examples of the received constellation diagrams for the subcarriers n_1 and n_5 for $L_s = 10$ and $\beta = 0.2$) showing the significant increment in the system complexity in comparison with 2- and 6-CAP links.

Finally, the summary of the highest measured R_b and η_{se} as well as corresponding L_s and L_f for $m = \{2, 4, 6, 8, 10\}$ for $B_{sig} = 1$ MHz and 2 MHz are given in Tables 2 and 3, respectively. Note that, the results for 4-CAP are given as well, although we did not discussed them since they display similar performance to the other *m*-CAP systems. For $B_{sig} = 1$ MHz the highest improvement in

TABLE 2
The Highest Measured Bit Rates and Spectral Efficiencies for the Signal Bandwidth 1 MHz

m	**2**	**4**	**6**	**8**	**10**
R_b (Mb/s)	6.50	7	7	7.13	7
L_s (symbols) / β	10 / 0.8	10 / 0.8	10 / 0.2	10 / 0.2	10 / 0.2
L_f (taps/filter)	161	301	301	401	481
η_{se} (b/s/Hz)	4.23	5	5.83	5.94	5.83
L_s (symbols) / β	10 / 0.3	10 / 0.2	10 / 0.2	10 / 0.2	10 / 0.2
L_f (taps/filter)	121	201	301	401	481

TABLE 3
The Highest Measured Bit Rates and Spectral Efficiencies for the Signal Bandwidth 2 MHz

m	**2**	**4**	**6**	**8**	**10**
R_b (Mb/s)	9.8	10.5	11.33	12.25	11.6
L_s (symbols) / β	10 / 0.8	10 / 0.8	10 / 0.4	10 / 0.2	10 / 0.2
L_f (taps/filter)	161	301	341	401	481
η_{se} (b/s/Hz)	3.7	4	4.31	5.1	4.83
L_s (symbols) / β	10 / 0.3	10 / 0.2	10 / 0.2	10 / 0.2	10 / 0.2
L_f (taps/filter)	121	201	301	401	481

R_b is 9.69%, i.e. from 6.50 Mb/s (2-CAP) to 7.13 Mb/s (8-CAP). For $m > 4$ the improvement in measured R_b is negligible, which is attributed to the fact that increasing m (i.e., decreasing the bandwidth requirement of individual subcarriers) does not lead to further improvement in the flat-band approximation of the LED frequency response, and hence higher SNR values cannot be achieved. Note that, η_{se} is improved by 40.43% from 4.23 b/s/Hz (2-CAP) to 5.94 b/s/Hz (8-CAP), which is significant. However, this improvement comes at the cost of increased number of filter taps (i.e., system complexity). Improvement in R_b can be showed when considering higher $B_{sig} = 2$ MHz but at the cost of reduced η_{se} as given in Table 3. For higher order systems with $m \geq 6$ the same filter parameters can be adopted in order to optimize the system design to achieve both maximum R_b and η_{se}. To increase further both R_b and η_{se} in a point-to-point VLC system, pre- and post-equalization schemes (hardware or software) should be adopted.

4. Conclusion

In this work, we experimentally tested *m*-CAP system performance for different parameters of the FIR filters that introduce major complexity in a VLC system. We showed that both filter parameters L_s and β have a significant impact on the measured R_b and η_{se}. We achieved an improvement of 9.69% and 40.43% in the measured R_b and η_{se}, respectively, when compared 2-CAP and 8-CAP systems. The low order *m*-CAP schemes can be utilized providing the similar link R_b and η_{se} as higher

order systems and having much lower filter taps requirement (e.g., $L_f = 201$ and 401 taps/filter for $m = 4$ and 8, respectively). Contrary, the higher order systems with $m \geq 6$ can be designed to offer both the highest transmission speed and spectral efficiency using the same filter parameters (e.g., 8-CAP with $L_s = 10$ and $\beta = 0.2$).

References

[1] Cisco, San Jose, CA, USA, "Cisco visual networking index: Global mobile data traffic forecast update, 2016–2021 white paper," 2017.

[2] Z. Ghassemlooy, L. N. Alves, S. Zvanovec, and M. A. Khalighi, *Visible Light Communications Theory and Applications*. Boca Raton, FL, USA: CRC Press, 2017.

[3] J. Grubor, S. C. J. Lee, K. D. Langer, T. Koonen, and J. W. Walewski, "Wireless high-speed data transmission with phosphorescent white-light LEDs," in *Proc. 33rd Eur. Conf. Exhib. Opt. Commun.*, Berlin, Germany, 2007, pp. 1–2.

[4] X. Li *et al.*, "Wireless visible light communications employing feed-forward pre-equalization and PAM-4 modulation," *J. Lightw. Technol.*, vol. 34, no. 8, pp. 2049–2055, Apr. 2016.

[5] H. Le Minh *et al.*, "100-Mb/s NRZ visible light communications using a postequalized white LED," *IEEE Photon. Technol. Lett.*, vol. 21, no. 15, pp. 1063–1065, Aug. 2009.

[6] S. Rajbhandari, "Spatial and wavelength division multiplexing for high-speed VLC systems: An overview," in *Proc. 10th Int. Symp. Commun. Syst., Netw. Digital Signal Process.*, Prague, Czech Republic, 2016, pp. 1–6.

[7] F.-M. Wu, C.-T. Lin, C.-C. Wei, C.-W. Chen, Z.-Y. Chen, and H.-T. Huang, "3.22-Gb/s WDM visible light communication of a single RGB LED employing carrier-less amplitude and phase modulation," in *Proc. Opt. Fiber Commun. Conf. Expo. Nat. Fiber Opt. Eng. Conf.*, Anaheim, CA, USA, 2013, pp. 1–3.

[8] S. D. Dissanayake and J. Armstrong, "Comparison of ACO-OFDM, DCO-OFDM and ADO-OFDM in IM/DD systems," *J. Lightw. Technol.*, vol. 31, no. 7, pp. 1063–1072, Apr. 2013.

[9] J. Armstrong, "OFDM for optical communications," *J. Lightw. Technol.*, vol. 27, no. 3, pp. 189–204, Feb. 2009.

[10] R. X. G. Ferreira *et al.*, "High bandwidth GaN-based micro-LEDs for multi-Gb/s visible light communications," *IEEE Photon. Technol. Lett.*, vol. 28, no. 19, pp. 2023–2026, Oct. 2016.

[11] G. Cossu, W. Ali, R. Corsini, and E. Ciaramella, "Gigabit-class optical wireless communication system at indoor distances (1.5–4 m)," *Opt. Exp.*, vol. 23, pp. 15700–15705, 2015.

[12] D. Bykhovsky and S. Arnon, "An experimental comparison of different bit-and-power-allocation algorithms for DCO-OFDM," *J. Lightw. Technol.*, vol. 32, no. 8, pp. 1559–1564, Apr. 2014.

[13] H. Elgala, R. Mesleh, and H. Haas, "Nonlinearity effects and predistortion in optical OFDM wireless transmission using LEDs," *Int. J. Ultra Wideband Commun. Syst.*, vol. 1, no. 2, pp. 143–150, 2009.

[14] W. O. Popoola, Z. Ghassemlooy, and B. G. Stewart, "Pilot-assisted PAPR reduction technique for optical OFDM communication systems," *J. Lightw. Technol.*, vol. 32, no. 7, pp. 1374–1382, Apr. 2014.

[15] V. Guerra, C. Suarez-Rodriguez, O. El-Asmar, J. Rabadan, and R. Perez-Jimenez, "Pulse width modulated optical OFDM," in *Proc. IEEE Int. Conf. Commun. Workshop*, 2015, pp. 1333–1337.

[16] K. Weiwei and S. Hranilovic, "Power reduction techniques for multiple-subcarrier modulated diffuse wireless optical channels," *IEEE Trans. Commun.*, vol. 56, no. 2, pp. 279–288, Feb. 2008.

[17] F. M. Wu *et al.*, "Performance comparison of OFDM signal and CAP signal over high capacity RGB-LED-based WDM visible light communication," *IEEE Photon. J.*, vol. 5, no. 4, Aug. 2013, Art. no. 7901507.

[18] Y. Wang, L. Tao, X. Huang, J. Shi, and N. Chi, "8-Gb/s RGBY LED-based WDM VLC system employing high-order CAP modulation and hybrid post equalizer," *IEEE Photon. J.*, vol. 7, no. 6, Dec. 2015, Art. no. 7904507.

[19] M. I. Olmedo *et al.*, "Multiband carrierless amplitude phase modulation for high capacity optical data links," *J. Lightw. Technol.*, vol. 32, no. 4, pp. 798–804, Feb. 2014.

[20] P. A. Haigh *et al.*, "A multi-CAP visible-light communications system with 4.85-b/s/Hz spectral efficiency," *IEEE J. Sel. Areas Commun.*, vol. 33, no. 9, pp. 1771–1779, Sep. 2015.

[21] P. A. Haigh *et al.*, "Multi-band carrier-less amplitude and phase modulation for bandlimited visible light communications systems," *IEEE Wireless Commun.*, vol. 22, no. 2, pp. 46–53, Apr. 2015.

[22] K. Werfli *et al.*, "Multi-band carrier-less amplitude and phase modulation with decision feedback equalization for bandlimited VLC systems," in *Proc. 4th Int. Workshop Opt. Wireless Commun.*, Istanbul, Turkey, 2015, pp. 6–10.

[23] P. A. Haigh *et al.*, "Experimental verification of visible light communications based on multi-band CAP modulation," in *Proc. 2015 Opt. Fiber Commun. Conf. Exhib.*, Los Angeles, CA, USA, 2015, pp. 1–3.

[24] P. Chvojka, S. Zvanovec, K. Werfli, P. A. Haigh, and Z. Ghassemlooy, "Variable *m*-CAP for bandlimited visible light communications," in *Proc. IEEE Int. Conf. Commun. Workshops*, Paris, France, 2017, pp. 1–5.

[25] K. Werfli, P. A. Haigh, Z. Ghassemlooy, N. B. Hassan, and S. Zvanovec, "A new concept of multi-band carrier-less amplitude and phase modulation for bandlimited visible light communications," in *Proc. 10th Int. Symp. Commun. Syst., Netw. Digital Signal Process.*, Prague, Czech Republic, 2016, pp. 1–5.

[26] P. A. Haigh *et al.*, "Multi-band carrier-less amplitude and phase modulation for highly bandlimited visible light communications—Invited paper," in *Proc. Int. Conf. Wireless Commun. Signal Process.*, Nanjing, China, 2015, pp. 1–5.

[27] P. Chvojka, P. A. Haigh, S. Zvanovec, P. Pesek, and Z. Ghassemlooy, "Evaluation of multi-band carrier-less amplitude and phase modulation performance for VLC under various pulse shaping filter parameters," in *Proc. 13th Int. Joint Conf. e-Bus. Telecommun. Vol. 3, OPTICS*, Lisbon, Portugal, 2016, pp. 25–31.

[28] J. G. Proakis, *Digital Communications*. New York, NY, USA: McGraw-Hill, 2004.